Accessing Improbable Foldamer Shapes with Strained Macrocycles

Ko Urushibara,[a, b] Yann Ferrand,*[b] Zhiwei Liu,[c] Kosuke Katagiri,[d] Masatoshi Kawahata,[e] Estelle Morvan,[f] Ryan D'Elia,[c] Vojislava Pophristic,[c] Aya Tanatani,*[a] and Ivan Huc*[b, g]

Abstract: The alkylation of some secondary amide functions with a dimethoxybenzyl (DMB) group in oligomers of 8-amino-2-quinolinecarboxylic acid destabilizes the otherwise favored helical conformations, and allows for cyclization to take place. A cyclic hexamer and a cyclic heptamer were produced in this manner. After DMB removal, X-ray crystallography and NMR show that the macrocycles adopt strained conformations that would be improbable in noncyclic species. The high helix folding propensity of the main chain is partly expressed in these conformations, but it remains frustrated by macrocyclization. Despite being homomeric, the macrocycles possess inequivalent monomer units. Experimental and computational studies highlight specific fluxional pathways within these structures. Extensive simulated annealing molecular dynamics allow for the prediction of the conformations for larger macrocycles with up to sixteen monomers.

Introduction

Macrocyclization is intimately linked to the stabilization of molecular shape.[1] In flexible backbones, it helps to reduce conformational space and thus promotes conformations that are accessible to noncyclic precursors, but that may be disfavored for entropic reasons because they compete with multiple alternate stable states. Disulfide bridge formation in native protein structures and stapling of α-helical peptides[2] or proteins[3] typically illustrate this effect. Folded macrocycles with multiple aromatic rings are another illustration.[4] In contrast with the above, the so-called shape-persistent macrocycles consist of rigid subunits and generally have structures close to those of their related noncyclic precursors (Scheme 1a).[1,5–7] Their synthesis is often high yielding, even when it entails the oligomerization of multiple units. Shape-persistent macrocycles are frequently flat, rigid, aryl-containing rings, and often display interesting aggregation properties.[8] A third category of macrocycles are those that are inherently strained. Strain generates constraints that reduce conformational freedom. It thus also stabilizes macrocycle shape but these shapes are spring loaded and by definition enthalpically disfavored in noncyclic precursors. Interest for strained rings has for long focused on small cycles with less than ten atoms because they display unusual reactivity and constitute desirable yet challenging synthetic targets.[9] In recent years, various strained macrocycles have been produced as well. Typical examples include cycloparaphenylenes,[10] cycles bearing angle strain alkynes,[11] and hydrocarbon belts.[12] In most cases, the synthetic approach involves the cyclization of a non-strained shape-persistent precursor, and subsequent irreversible transformations that change ring shape and introduce the strain.

[a] Dr. K. Urushibara, Prof. A. Tanatani
Department of Chemistry, Faculty of Science
Ochanomizu University
2-1-1 Otsuka, Bunkyo-ku,Tokyo 112-8610 (Japan)
E-mail: tanatani.aya@ocha.ac.jp

[b] Dr. K. Urushibara, Dr. Y. Ferrand, Prof. I. Huc
CBMN (UMR 5248)
Université de Bordeaux, CNRS, Bordeaux Institut National Polytechnique
2 rue Robert Escarpit, 33600 Pessac (France)
E-mail: y.ferrand@iecb.u-bordeaux.fr

[c] Prof. Z. Liu, R. D'Elia, Prof. V. Pophristic
Department of Chemistry & Biochemistry
University of the Sciences
600 South 43rd Street, Philadelphia, PA 19104 (USA)

[d] Dr. K. Katagiri
Department of Chemistry, Faculty of Science and Engineering
Konan University
8-9-1 Okamoto, Higashinada-ku, Kobe, 658-8501 (Japan)

[e] Dr. M. Kawahata
Faculty of Pharmaceutical Sciences
Showa Pharmaceutical University
3-3165 Higashi-Tamagawagakuen, Machida, Tokyo 194-8543 (Japan)

[f] E. Morvan
IECB (UMS3033/US001)
Université de Bordeaux, CNRS, INSERM
2 rue Robert Escarpit, 33600 Pessac (France)

[g] Prof. I. Huc
Department of Pharmacy and Center for Integrated Protein Science
Ludwig-Maximilians-Universität
Butenandtstr. 5–13, 81377 München (Germany)
E-mail: ivan.huc@cup.lmu.de
Homepage: https://huc.cup.uni-muenchen.de/

Supporting information for this article is available on the WWW under https://doi.org/10.1002/chem.202101201

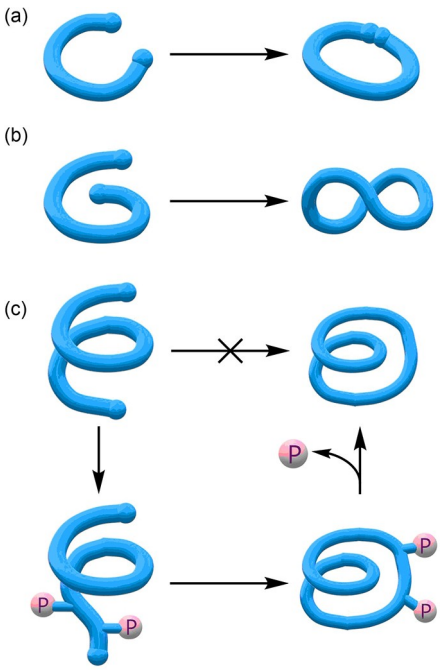

Scheme 1. (a) The ends of a crescent-shape precursor may react to produce a shape-persistent macrocycle. (b) When the precursor is a helix spanning not much more than one turn, cyclization may still occur and entail some distortion, for example, a saddle-shape structure. (c) The ends of a longer helix may not meet, but the introduction of disruptors of helicity (P groups) allow for cyclization. A constrained macrocycle is obtained after removal of the P groups.

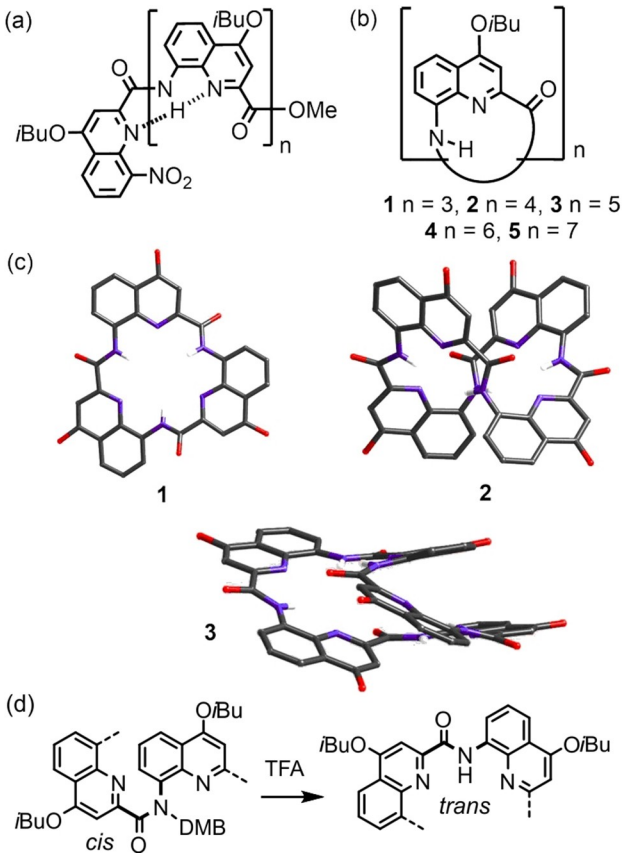

Figure 1. Chemical structures of (a) non cyclic 8-amino-2-quinolinecarboxylic acid oligoamides, and (b) macrocycles **1**–**5**. (c) Crystal structures of **1**–**3** shown at the same scale.[7,17] Included solvent molecules, isobutyl groups, and protons other than amide NHs have been removed for clarity. (d) *Cis* to *trans* amide conformational transition upon removing a dimethoxybenzyl group (DMB) from an aromatic amide bond.

The resulting strain arises from the bending of rigid building blocks that would not be curved if the ring was cut open. With very large, less strained rings, using templates produces the desirable ring size.[13]

Here, we extend the concept of using strained macrocycles to generate otherwise inaccessible molecular shapes, by taking advantage of folding frustration. Considering a molecule that adopts a well-defined folded conformation, the creation of a short covalent linkage between two parts of the molecule that are remote in space in the native fold will forbid this particular fold. If the molecule's folding propensity is weak, we anticipate that this destabilization of the native fold is unlikely to produce a new structurally well-defined object. However, in a system where folding propensity is strong, we expect that the conformational frustration arising from the cyclization will result in one, possibly more, alternate stable conformations that could not be produced in a noncyclic structure. Because of their particularly strong folding propensity, aromatic amide foldamers[14] are ideal candidates to explore this concept.

Many aromatic oligoamides possess an inherent curvature that has been exploited to produce shape persistent macrocycles,[15] and that results in helical structures if a noncyclic sequence is extended beyond one turn. Oligomers of 8-aminoquinolinecarboxylic acid Q (Figure 1a) adopt a particularly stable helical conformation in essentially any solvent.[16] These conformations are promoted by the pseudo-conjugation between sp^2-hybridized amide groups and quinoline rings, by electrostatic repulsions between amide oxygen atoms and neighboring quinoline endocyclic nitrogen atoms, and by bifurcated hydrogen bonds between amide NH and adjacent quinoline nitrogen atoms. These interactions give rise to a natural curvature of 2.5 units per turn. With minimal distortion, shape-persistent trimeric macrocycle **1** can be obtained (Figure 1b,c).[7] Tetramer **2** naturally spans more than 1.5 helix turns. Under conditions that destabilize the helix (heat and concentrated LiCl), it can nevertheless be cyclized into a saddle-shape object with S_4 symmetry (Scheme 1b, Figure 1b,c), which stood as a first illustration of our concept.[7]

However, longer Q_n helices are extremely stable (e.g. even in TFA) and no denaturing conditions have been reported until now. Joining the diverging ends of these longer helices to form larger homomeric macrocycles does not occur spontaneously. In a recent report,[17] we showed that the introduction of removable 2,4-dimethoxybenzyl (DMB) substituents on some amide nitrogen atoms disrupted the helix, allowing for the cyclization of a pentamer in the same series (Scheme 1c). After DMB removal, pentamer **3** was produced and characterized (Figure 1c,d). Conformational frustration in **3** is expressed by the occurrence of a disfavored *cis* secondary amide.[18] In the

following we show that the same strategy may be applied to produce hexamer **4** and heptamer **5**. In both cases, original, compact structures are obtained that differ much from the noncyclic helices and that undergo complex fluxional behaviors. In addition, computational investigations allowed us to make plausible hypotheses about the conformational behavior of longer sequences with up to sixteen units. Given the variety of monomers and linkages that can be introduced in aromatic foldamer backbones, the breadth of systems to which this approach may be applied is considerable. Innumerable original molecular shapes may thus be accessed, which would not be significantly populated in noncyclic molecules.

Results and Discussion

Macrocycle synthesis

DMB groups have been used as removable amide conformational disruptors in solid phase peptide synthesis to prevent aggregation or folding on the solid support.[19] Similarly, they have been used to disrupt aggregation and thus enhance the solubility of Kevlar-like oligomers of 4-amino benzoic acid, thus allowing for their functionalization prior to DMB removal.[20] The alkylation of amides derived from an aromatic acid and an aromatic amine favors an unusual *cis* orientation of the two aryl rings, in sharp contrast with the *trans* conformation of the secondary amide precursors,[21] a property that has been exploited to generate original tertiary amide and tertiary urea foldamers.[22] If the alkyl group is removable, like the acid labile DMB, its insertion or removal results in a radical change of conformational preference. We have previously taken advantage of this conformation change to produce cyclic pentamer **3** from noncyclic precursors containing two DMB groups.[17] In order to produce the equivalent hexameric and heptameric macrocycles, a series of noncyclic precursors **6** and **7** was synthesized (Scheme 2, see Supporting Information for synthetic Schemes and experimental procedures). We found that cyclization failed for all sequences containing a single DMB group and for **6b** which contains two consecutive DMB groups at the *C*-terminus. In contrast, all precursors containing two DMB groups within their sequence could be converted into the corresponding macrocycles **8c**, **8d**, and **9b** in moderate to good yield.

The solid state structures of all three products were obtained by X-ray diffraction analysis on single crystals (Figure 2a–2c). The three macrocycles contain in total six DMB-substituted amides (two per product), of which five adopt the expected *cis* conformation (shown in purple in Figure 2), and one is *trans* (Figure 2a). The structures also reveal two flipped amides per structure (shown in green in Figure 2), that is, amide functions that deviate from the preferred conformation shown in Figure 1a. These amide groups may for example be perpendicular to an adjacent quinoline or with the carbonyl oxygen atom pointing towards – instead of away from – a neighboring endocyclic quinoline nitrogen atom.

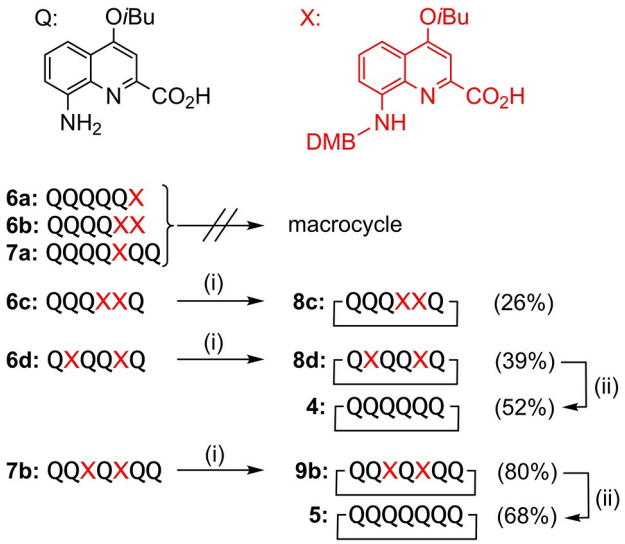

Scheme 2. Macrocyclization of quinolinecarboxamide oligomers of different lengths bearing DMB groups at various amides, and subsequent DMB deprotection. Conditions: (i) PPh_3, trichloroacetonitrile, DIPEA, $CHCl_3$; (ii) TFA (neat), 60 °C. DMB: 2,4-dimethoxybenzyl.

The ^{1}H NMR spectra of **8c** and **9b** both show two sets of signals that indicate that at least one conformer exists in solution in addition to the conformer observed in the solid state. Of note is the simple NMR spectrum of **8d** (Figure 2e) which matches with its C_2-symmetrical solid state structure conformation. These various conformers were not investigated further. They presumably represent conformations close to the conformers conducive to cyclization. The presence of flipped amides within these conformers suggests that some conformational distortion was necessary for cyclization, in addition to the DMB-induced *cis* amide bonds. This makes it difficult to accurately predict which precursor may be prone to cyclization and which may not. Nevertheless, the results shown in Scheme 2 provide useful empirical guidelines.

The final removal of the DMB groups in neat TFA yielded **4** and **5**, the structure and dynamics of which were investigated as follows.

Structure analysis and conformational dynamics of cyclic hexamer 4

The solid state structure of **4** could also be obtained by single crystal X-ray diffraction (Figure 3a). The conformation has an average – non crystallographic – center of symmetry. It contains two helix segments with opposite *P* and *M* handedness linked "head to tail" by two extended (E) segments. Each E segment has two adjacent flipped amides (in green in Figure 3a), so there is a total of four flipped amides out of six in the structure. This highlights how far this object is from a canonical Q_n helix. Its conformation would be extremely unstable if not constrained in a macrocycle. We denote this conformation as

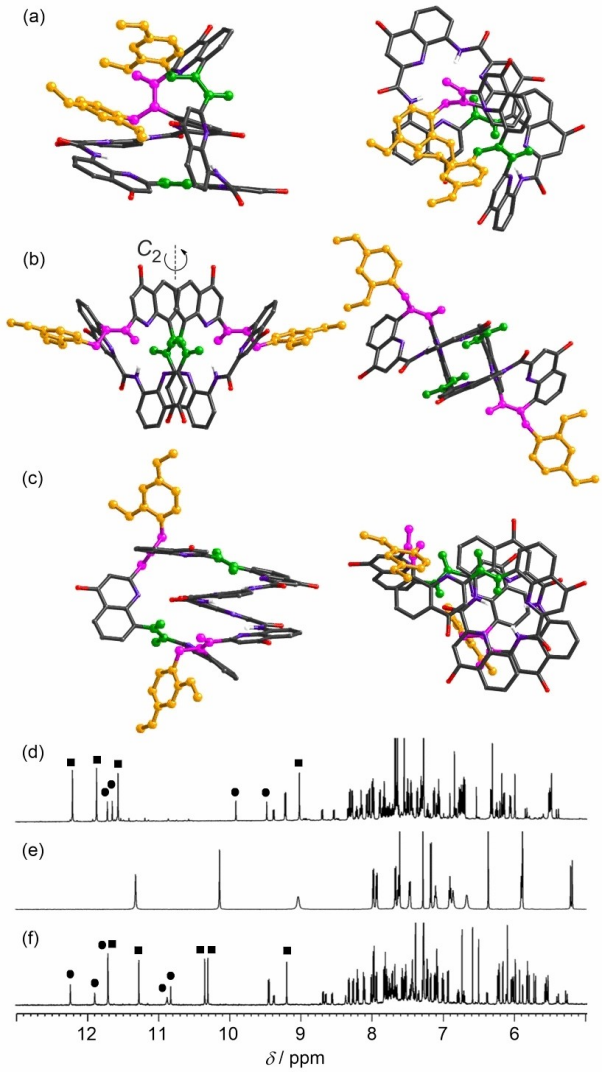

Figure 2. Views of the X-ray crystal structures of: (a) **8c**, (b) **8d** and (c) **9b**. DMB groups are shown in orange ball and stick representation. The *cis* and flipped amide groups are marked with magenta and green balls, respectively. Hydrogen atoms other than NH, isobutyl side chains, and solvent molecules have been removed for clarity. Part of the 600 MHz ^{1}H NMR spectra at 298 K of (d) **8c**, (e) **8d** and (f) **9b** in $CDCl_3$. Amide NH protons, major and minor conformers are marked with filled squares (■) and filled circles (●), respectively.

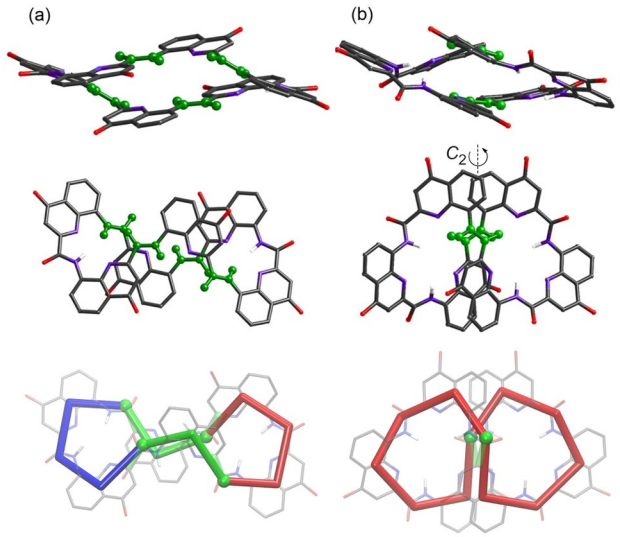

Figure 3. (a) Views of the ME_2PE_2 X-ray crystal structure of **4** and (b) snapshot of another stable species (M_2EM_2E) found in MD simulations of **4**. Hydrogen atoms other than NH, isobutyl chains, and solvent molecules have been removed for clarity. From top to bottom are side views, top views and tube representations of the conformers. The vertices of the tube representation connect centers of mass of the quinoline and the amide units. Red, blue and green tubes/balls represent left-handed (*M*), right-handed (*P*) and extended sections (flipped amide, E), respectively.

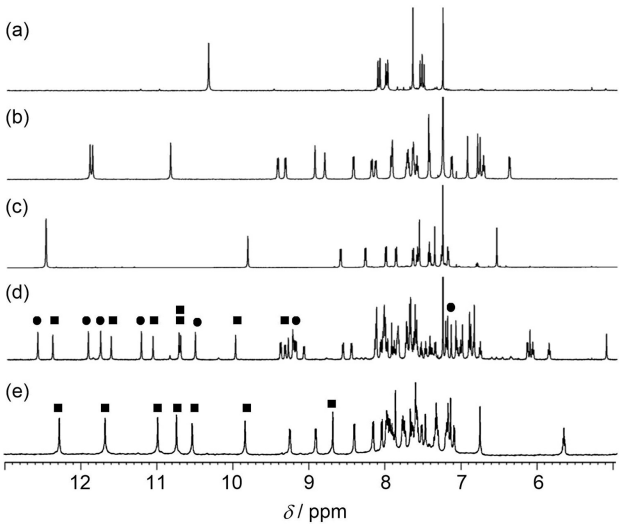

Figure 4. Part of the 600 MHz ^{1}H NMR spectra at 298 K of (a) **2**, (b) **3**, (c) **4** and (d) **5** in $CDCl_3$ and of (e) **5** in DMSO-d_6, showing amide and aromatic resonances. Black circles and squares indicate NH resonances of two distinct conformers in the spectra of **5**.

ME_2PE_2, in which each letter indicates the *M* (red), *P* (blue), or E (green) folding pattern of a Q–Q linkage.

The ^{1}H NMR spectrum indicates that hexameric **4** has a symmetrical structure with three inequivalent rings in solution as well (Figure 4c), in agreement with its solid state structure. This partial symmetry contrasts with the ^{1}H NMR spectrum of **2**, which shows that all rings are equivalent in the tetramer (Figure 4a), and with that of **3** which shows that that all five rings are inequivalent in the pentamer (Figure 4b). In parallel, the conformation of **4** was assessed using molecular dynamics (MD) simulations (see Supporting Information for details). The simulations identified the solid state ME_2PE_2 structure as a populated species (Figure 3a), but they also revealed a second major conformer with an M_2EM_2E (or P_2EP_2E) structure (Figure 3b). The M_2EM_2E conformer possesses an average C_2 symmetry axis and thus three inequivalent rings. Remarkably, it contains only two energetically disfavored flipped amides (dihedral N_{Ar}-C_{Ar}-C_{Am}-N_{Am} angle ≈180°) and thus also stands as a plausible candidate for a stable conformer. This observation called for a validation of the solution structure of **4**.

The elucidation of the folded structure of **4** (in CD_2Cl_2 at 258 K where signals were particularly well resolved) was made possible by using a combination of 2D NMR techniques including ^{1}H-^{1}H COSY, ^{1}H-^{13}C HSQC, ^{1}H-^{13}C HMBC and ^{1}H-^{1}H ROESY (Figures S1-S5). The assignment of a large part of the ^{1}H and ^{13}C spectra (i.e. excluding some side chain protons) is reported in the Supporting Information (Table S1). NOE correlations, including strong correlations between the N*H* of flipped amides and neighboring aromatic protons (Figure S5) support the prevalence in solution of the structure observed in the solid state and exclude the computed conformer found only in MD simulations (Figure 3b).

The fluxional behavior of **4** was also investigated by MD simulations. Twelve simulations with different initial structures bearing structural characteristics of either ME_2PE_2 or M_2EM_2E were carried out for a total simulation time of ~3 μs. Each simulation consisted of multiple heating/cooling cycles at up to 800 K. The observation of the ME_2PE_2 or M_2EM_2E conformer in each MD trajectory is exclusive, i.e. no interconversion between the two was observed, which precluded an assessment of their relative stability by means of sampling different populations of conformers. Ab initio optimizations in the gas phase were undertaken at the B3LYP/6-31 g(d) level taking two snapshots from MD as initial structures, but they also remained inconclusive in this respect, because they are not representative of the multiple local minima observed during MD simulations, and because they do not provide solvation energy and entropic terms.

The MD simulations showed that the six degenerate conformations of ME_2PE_2 form two groups of three conformers that are only convertible within the group as two independent fluxional processes. We denote the degenerate states as M_iP_{i+3} (or P_iM_{i+3}) in which i and i + 3 indicate the central position of the two helical segments with *M* or *P* labelling handedness of the segment, respectively. The interconversion follows the $M_iP_{i+3} \leftrightarrow P_{i+1}M_{i+4} \leftrightarrow M_{i+2}P_{i+5} \leftrightarrow P_{i+3}M_{i+6}$ (which is M_iP_{i+3}) path or the mirroring $P_iM_{i+3} \leftrightarrow M_{i+1}P_{i+4} \leftrightarrow P_{i+2}M_{i+5} \leftrightarrow M_{i+3}P_{i+6}$ (which is P_iM_{i+3}) path. On average, four interconversions occur within ten heating/cooling cycles and the transition is quick and clean with no lingering intermediates. As a result, the ME_2PE_2 conformers account for ~96% of the total ensemble of MD trajectories at T = 300 K (920 ns). The frequency of interconversion indicates that the degenerate states are separated by a modest barrier and are close to each other in the conformational space. Furthermore, the ~96% population indicates steep minima, and thus stiff conformers.

The absence of interconversion between ME_2PE_2 and M_2EM_2E conformers during the MD trajectories despite the high in silico temperatures involved hint at a high kinetic barrier between them. One could thus hypothesize that the observed ME_2PE_2 conformer is in fact a kinetically trapped conformation. Though this hypothesis cannot be formally excluded, we note that the TFA treatment of the two different DMB-protected precursors **8c** and **8d** yielded the same ME_2PE_2 conformer of **4**, i.e. that this conformer can be produced by different conformation pathways.

Structure analysis of cyclic heptamer 5

The crystal structure of heptamer **5** reveals an unprecedented miniature helix-loop motif (Figure 5a). The structure contains only two flipped amides. The macrocycle is thus large enough to allow a sufficient number of monomers to fulfill their potential for noncovalent interactions and thus form two helical turns. This helix-loop conformation resembles that of the DMB-substituted precursor **9b** (Figure 2c), except that the latter contained two *cis* amides in addition to two flipped amides. The ^{1}H NMR spectrum of **5** in DMSO-d_6 shows a single species with seven inequivalent quinoline rings, which indicates that fluxional behavior is slow on the NMR time scale (Figure 4e). In contrast, in $CDCl_3$, two species in comparable proportions were observed (Figure 4d), both with seven inequivalent monomers. Spectra in solvent mixtures allowed us to assign one of the two $CDCl_3$ species to the one that prevails in DMSO (Figure S7). A ^{1}H-^{15}N HSQC spectrum shows that the second species in $CDCl_3$ has an unusually upfield shifted amide at 7.20 ppm. This value is much lower than what is expected for hydrogen bonded amides, and even for flipped amides (Figure 2a, 2c), making it in unlikely that this conformer corresponds to that observed in the solid state. Thus, the solid state structure more likely corresponds to the species that prevails in DMSO.

Twenty-five MD simulations of macrocycle **5** were then carried out, starting from different initial structures, each with multiple heating/cooling cycles (Table 1). The total ensemble of MD trajectories amounted to 8 μs. A major conformer, M_4EME

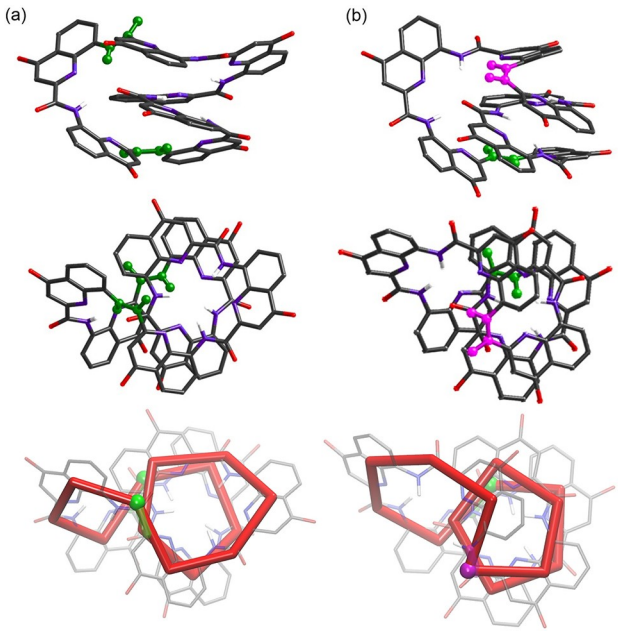

Figure 5. (a) Views of the M_4EME X-ray crystal structures of **5** and (b) snapshot of a higher energy M_3CM_2E conformation found in MD simulations of **5**. Hydrogen atoms other than NH, isobutyl chains, and solvent molecules are removed for clarity. From top to bottom are side view, top view and tube representation. The vertices of the tube representation connect centers of mass of the quinoline and the amide units. Red, blue, green and magenta tubes/balls represent left-handed (*M*), right-handed (*P*), extended sections (flipped amides, E), and *cis* amide (C), respectively.

Table 1. Macrocycle conformations at the start and end of MD annealing simulations.

Qn macrocycle size	Starting conformation	Number of simulations	Total simulation time (ns)	Final conformational distributions[a]
6mer (**4**)	M_2EM_2E	7[b]	1120	M_2EM_2E (71 %[c] + 26 %[d])
	ME_2PE_2	5	1840	**ME_2PE_2** (96 %)
7mer (**5**)	M_4EME	25[e]	8000	**M_4EME** (70 %);[c] M_3CM_2E (4 %); *$ME_2P_2E_2$* (8 %)
8mer	M_4E_4	1	160	*M_4EM_2E* (61 %)
	M_4EM_2E	1	160	*M_4EM_2E* (66 %)
	ME_3ME_3	1	160	**MEP_2EPE_2** (99.9 %)
9mer	M_6E_3	1	80	$M_4E_2PE_2$ (99 %)
	$M_4E_2PE_2$	1	160	$M_4E_2PE_2$ (85 %)
10mer	M_6E_4	1	80	No stable structure
	M_4EM_4E	1	80	No stable structure
11mer	M_6E_5	1	80	**$M_6E_2PE_2$** (56 %); *M_6E_5* (39 %)
	$M_6E_2PE_2$	1	160	$M_6E_2PE_2$ (56 %); *M_6E_5* (40 %)
12mer	$M_4E_2P_4E_2$	1	320	**$M_4E_2P_4E_2$** (> 99.9 %)
	M_8E_4	1	80	$M_7E_2PE_2$ (53 %)
13mer	$M_6E_3ME_3$	1	80	$M_6E_3ME_3$ (75 %)
14mer	$M_6E_2P_4E_2$	1	160	**$M_6E_2P_4E_2$** (> 99.9 %)
	$M_4E_3M_4E_3$	1	80	$M_4E_3M_4E_3$ (> 99.9 %)
	$M_9E_2PE_2$	1	160	**M_9E_5** (99 %)
	M_9E_5	1	80	M_9E_5 (99 %)
16mer	$M_6E_2P_6E_2$	1	320	$M_6E_2P_6E_2$ (94 %)
	$M_6E_3M_4E_3$	1	200	**$M_6E_3M_4E_3$** (> 99.9 %)
	$M_9E_3ME_3$	1	80	$M_9E_3ME_3$ (75 %)

[a] M, P, C and E indicate left-handed, right-handed, *cis*-amide, and extended Q–Q linkages, respectively. Conformers in italics contain strongly fluctuating sections typical of intermediate structures. Conformers in bold are thought to be prevalent. Percent values are based on 300 K data only. Percentage includes all degenerate states of each conformer. [b] Seven different starting structures with various combinations of aryl-CO, aryl-NH and *cis*-amide misfolds at the two E sites. [c] Only aryl-CO misfolds. [d] With one or two aryl-NH misfolds. [e] Twenty-five starting structures with varying misfold types and degenerate states.

(or P_4EPE), was found; it corresponds to the helix-loop structure observed in the solid state and accounts for 70 % of the total ensemble of 300 K trajectories. Two other conformers, each accounting for less than 10 % of the total ensemble, were also identified. The first one, M_3CM_2E, is again a helix-loop conformer (Figure 5b). It differs from the major conformer notably by a *cis*-amide misfolding, noted as C. The second one, $ME_2P_2E_2$, resembles the centro-symmetrical ME_2PE_2 conformation of **4** (Figure 3a), with one extra monomer inserted in a helical section. The pattern and frequency of occurrence of these two conformers suggest that M_3CM_2E represents a stable (albeit minor) conformation, whereas $ME_2P_2E_2$ is more likely an intermediate along the conversion pathways. Indeed, M_3CM_2E occurs about ten times less frequently but each occurrence lasts seven times longer than those of $ME_2P_2E_2$. Furthermore, one or more $ME_2P_2E_2$ conformers always appears along any of the interconversion pathways between two helix-loop conformers, whereas M_3CM_2E does not. In addition, conformational fluctuation is much greater in $ME_2P_2E_2$, which is a characteristic of intermediate species.

Using a density functional theory (DFT) method (B3LYP/6-31G(d)//WP04/6-31G++(d,p)) and a continuum solvent model (chloroform), we calculated NMR chemical shift values of the different conformers of **5** after geometry optimization (see Table S2 and Figure S10). These calculations have limited predictive accuracy in the case of these large folded molecules involving extensive ring current effects, in contrast with other systems where they have been used effectively.[4b,c] For instance, tentatively matching unassigned signals between the calculated and observed spectra requires accommodation of chemical shift differences in the 0.5 to 1 ppm range. Nevertheless, one and only one high-field shifted amide NH signal at 8.05 ppm is predicted for the *cis* amide NH of the M_3CM_2E conformer. Since this is at least 3 ppm upfield-shifted from a normal value, we think that comparing observed and calculated signal is valid in this case. Thus, this makes it reasonable to propose that this conformer corresponds to the second species observed in NMR spectra in $CDCl_3$.

Fluxional behavior of cyclic heptamer 5

The main helix-loop conformer of **5** has fourteen degenerate states, seven for M_4EME and seven for the enantiomer P_4EPE. During MD simulations, interconversions between these degenerate conformers occurred via two pathways. A $M_i \leftrightarrow P_{i\pm1}$ chirality inversion pathway dominated. A $M_i \leftrightarrow M_{i\pm2}$ (or $P_i \leftrightarrow P_{i\pm2}$) chirality preservation pathway occurred about half as frequently. On average, 0.6 conversions were observed for every 10 heating/cooling cycles. The transition typically involved various intermediates.

In order to investigate this fluxional behavior experimentally, an analogue of Q bearing a fluorine atom in position 6 was synthesized and incorporated into **5F**, an analogue of **5** containing only one such unit (Figure 6a). Macrocycle **5F** thus differs from **5** by the replacement of one proton by a fluorine atom. Its conformers are no longer degenerate, save that each exists as a pair of enantiomers. As for **5**, only one conformer family is observed in DMSO, and two in $CDCl_3$. The ^{19}F NMR spectrum of **5F** in DMSO-d_6 shows seven peaks noted from A to

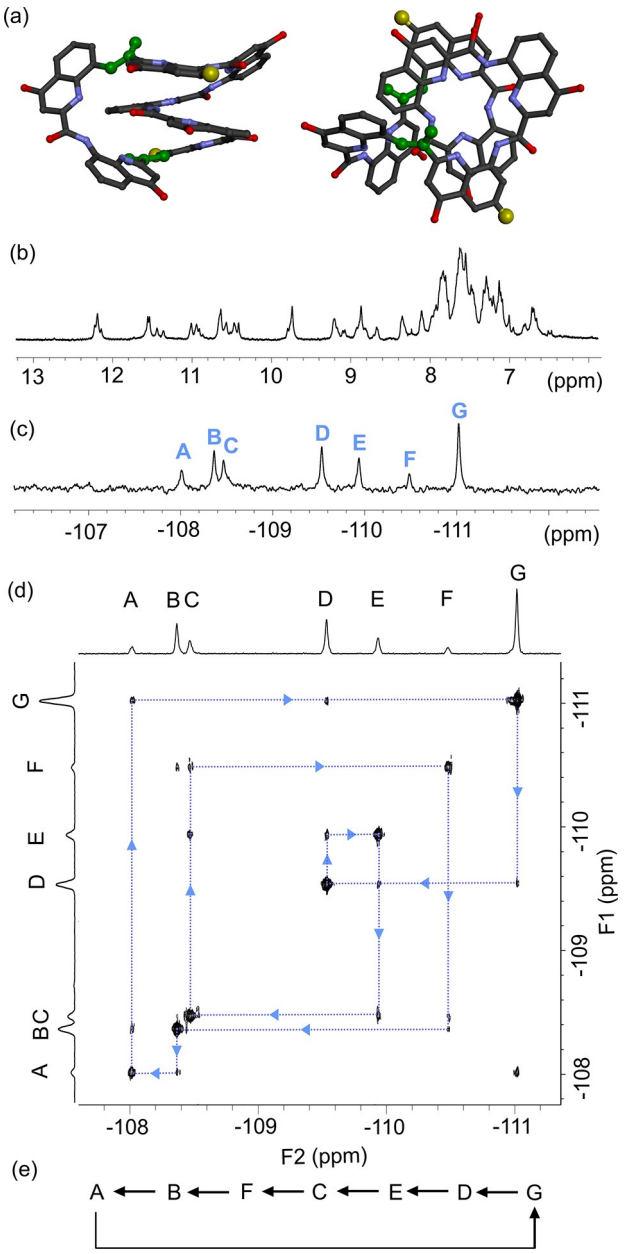

Figure 6. (a) Views of the X-ray crystal structures of **5F**. The flipped amide groups and fluorine atoms are marked with green and yellow balls, respectively. The fluorine atom is distributed over two sites in a 7/3 ratio. Hydrogen atoms other than NH, isobutoxy side chains, and solvent molecules have been removed for clarity. Part of the: (b) ^{1}H NMR (400 MHz) and (c) ^{19}F NMR (376 MHz) spectra of **5F** in DMSO-d_6 at 323 K. (d) ^{19}F EXSY spectrum (323 K, 376 MHz, mixing time 50 ms) showing chemical exchange between the different conformers. (d,e) Arrows denote the direction of the fluxional motion.

G in Figure 6c, that correspond to the seven conformers in which the fluorine is at one of the seven possible different sites of the folded conformation. Remarkably, the peaks do not have the same intensity, indicating that subtle energy changes result from placing the fluorine at one site or another.

The crystal structure of **5F** was solved (Figure 6a), and found to be similar to that of **5**. Structure refinement failed to converge when trying to model the electron density of the fluorine distributed over seven sites. This could be attributed to weak residual density that would amount to less than 10–20% of a fluorine atom. The structure converged when fluorine disorder was modeled over two sites in a 3/7 ratio; X-ray crystallography is less accurate than NMR in this matter and some positions with a low occupancy factors may have been overlooked. Moreover, the prevalence of conformers in the crystal lattice is influenced by crystal packing, not just by their proportions in solution. Nevertheless, the crystal structure corroborates the observation in solution that the seven conformers of **5F** are not equally populated.

Fast exchange on the NMR timescale between the conformers was not reached even at 110 °C. EXSY spectroscopy at 50 °C and variable mixing times revealed the existence of a dominant exchange pathway between the conformers (Figure 6d,e). Indeed each ^{19}F signal was found to exchange predominantly with two others in the following order: A↔B↔F↔C↔E↔D↔G↔A. Whether this pathway matches with one of the two observed in MD simulations could not be ascertained. Nevertheless, we find that MD simulations make quite reliable predictions of the macrocycle structures and thus think this is the case for the prediction of fluxional behavior.

Prediction of the conformations of larger macrocycles

The simulated annealing MD of cyclic hexamer **4** and heptamer **5** were carried out in parallel with different initial conformers or different degenerate states within one conformer (Table 1). Each simulation had an extensive time span. The analysis of structure and dynamics of **4** and **5** was thus based on a sampling of the conformational space sufficient to obtain meaningful information on conformational distributions and interconversion pathways.[23] Nevertheless, as sequence length increases, the occurrence of interconversion between degenerate conformers becomes less frequent: from four transitions per 100 ns for **4** to less than one transition per 100 ns for **5**. For macrocycles larger than a heptamer, sufficient sampling of the conformational space would require an impractical computational time. Fortunately, the study of the penta-,[17] hexa- and heptamer allowed us to establish certain rules and patterns of macrocycle conformations. We thus endeavored to predict reasonably stable structures for macrocyclic sequences from the octamer to the hexadecamer by designing different initial structures that follow these rules and patterns.

For each macrocycle, one or more starting structures were built with a minimal number of flipped amides. In the above hexa- and heptamer simulations, initial structures were built using three types of misfolds, at aryl-CO, aryl-NH, or amide bonds. However, all initial structures converged quickly to show that flipped aryl-CO bonds are the most energetically accessible misfolds, in agreement with earlier findings on the helix handedness inversion pathway of noncyclic Q_n oligomers.[24] Therefore, only aryl-CO misfolds were used to build the starting structures of longer macrocycles. No other misfolds were subsequently observed in the MD simulations. In the following,

we use *M*, *P*, or E notations as defined above. We found that ring size constrains the number of units that can be involved in each *P*, *M*, or E segment in a given macrocycle. In addition, the number of units in a given helical section determines the relative orientation of its *N* and *C*-termini and thus constrains the geometry through which these termini may be connected. Table 1 summarizes the starting conformations and the conformations after MD annealing for the different macrocycle sizes.

The M_xE_z helix-loop geometry was considered as a reasonable starting point for a number of macrocycles (M_4E_4, M_6E_3, M_6E_5, M_8E_4, and M_9E_5). Except for M_9E_5, this conformation evolved during MD simulations to introduce one or two *P* or *M* folded elements within the loop: M_4EM_2E (Figure 7a), $M_4E_2PE_2$ (Figure 7b), $M_6E_2PE_2$, $M_7E_2PE_2$. This sometimes went along with a shortening of the initial helix segment. Yet, M_x or P_x helical sections with x = 1,2 (i.e. that do not span one turn) sometimes stretch to retain an extended loop character, in order to match the height of the other helical section with two or more turns, as highlighted by the M_4EME conformation of **5** in the solid state (Figure 5a). Furthermore, these short helical sections may unfold as well: the two main 11mer conformations, M_6E_5 and $M_6E_2PE_2$, were found to interconvert frequently. The helix-loop motif thus emerged as a viable conformation for many of the ring sizes.

As an exception, the all-E-loop of M_9E_5 did not evolve during the simulations. A reason may be its genuine stability within its local conformational space, i.e. through folding/unfolding of one, or less than one, helix turn. Figure 7d (right) shows that the lateral length of the four-turn helix M_9 segment matches well with the length of the E_5 loop. Such genuine stability is supported by the fact that a simulation starting with $M_9E_2PE_2$, whose loop contains a *P* section, quickly converges back to M_9E_5. Two helix-helix conformers $M_6E_2P_4E_2$ or $M_4E_3M_4E_3$ are also found to be very stable by MD simulations (Table 1, Figure 7d). However, since no interconversion is observed, we cannot

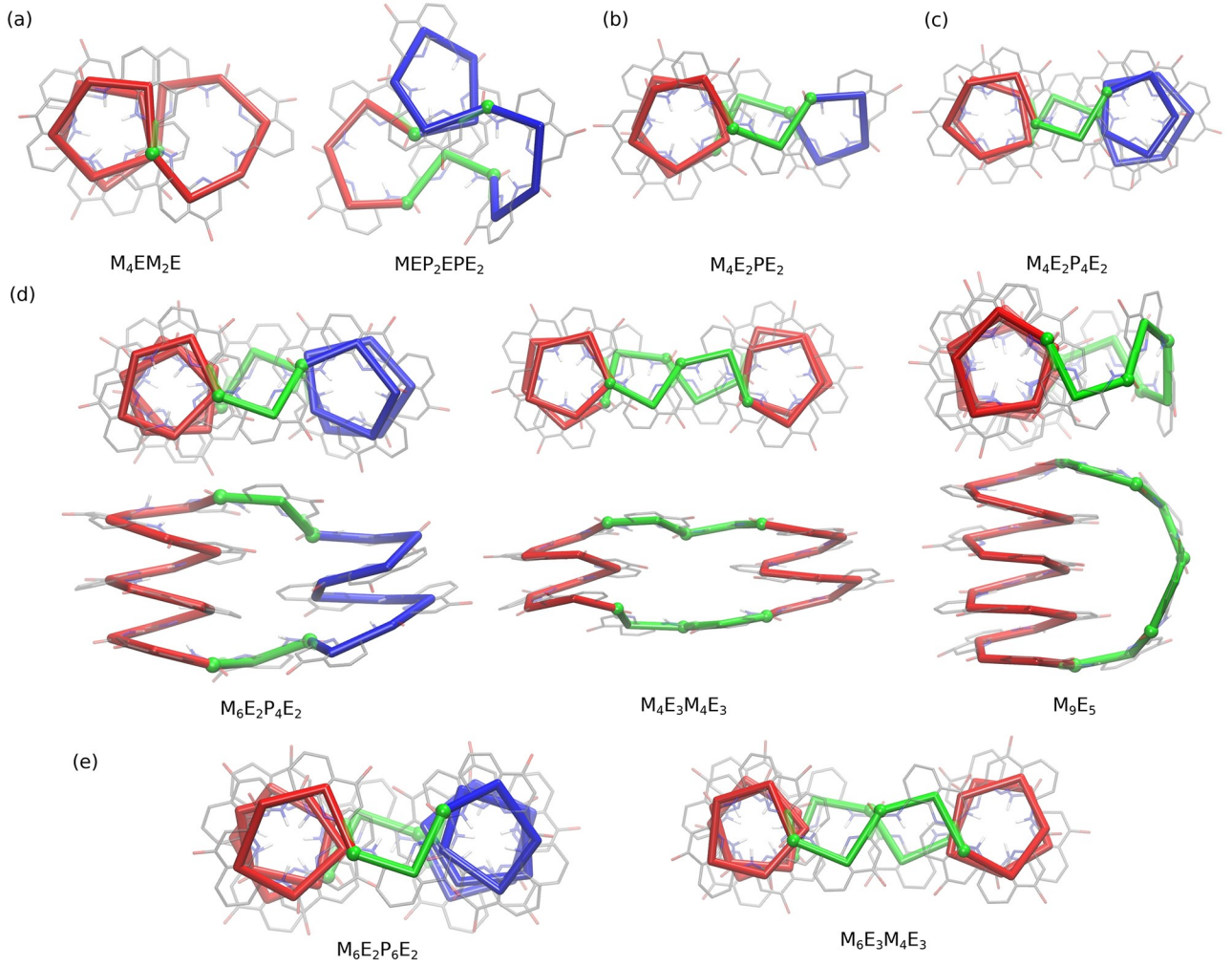

Figure 7. Conformations of larger Qn macrocycles as predicted by MD simulations. (a) 8mer. (b) 9mer. (c) 12mer. (d) 14mer top and side views. (e) 16mer. M, P, and E indicate left-handed, right-handed, and extended Q–Q linkages, respectively. For the structures shown in this figure, all E junctions entail a flipped secondary amide at an aryl-CO bond. Atomistic representations of the molecular structures are shown in light grey(C)/red(O)/blue(N)/white(H) (hydrogen atoms other than NH and isobutyl side chains omitted for clarity). Overlaid tube representations depict the overall geometry. The vertices of the tubes connect centers of mass of the quinoline and the amide units. Red, blue and green tubes represent left-handed (M), right-handed (P) and extended (E) sections, respectively.

assess the relative stability of the three conformers via sampling.

Also considered as starting structures were helix-helix conformations, i.e. conformations that contain two helical sections of three or more units. Annealing simulations showed an incredible stability of these conformers, that account for >99.9% of the populations at 300 K in several cases (Figure 7c,d,e). It should be noted that the observed conformational changes in simulations starting with M_xE_z (helix-loop) were limited to less than one helix turn (one or two units), whether it is folding of one or two extended units, or unfolding of one or two helical units. This is likely because the time span of each simulation was insufficient for folding and unfolding of longer sections. For example, the M_8E_4 starting structure evolved to $M_7E_2PE_2$ (53% population in the time ensemble) in 80 ns, but was not able to evolve to the $M_4E_2P_4E_2$helix-helix conformer. Though no direct conversion between $M_7E_2PE_2$ and $M_4E_2P_4E_2$ was observed, the fact that a simulation starting with $M_4E_2P_4E_2$ produces >99.9% population of $M_4E_2P_4E_2$ suggests that it is more stable.

These results point to several simple structural rules. First, when z is odd, an E_z segment connects two helices of identical handedness; when z is even, the segment connects two helices of opposite handedness. In a macrocycle with two E_z segments, z values must then both be odd or both be even. Since most stable conformers are obtained with low values of z, two main classes of reasonable conformers having monomeric E or dimeric E_2 segments were found by MD to be stable: M_xEM_yE (and its enantiomer) and $M_xE_2P_yE_2$ (and its enantiomer), marked here as Type I and Type II conformers, respectively. As seen above, hexamer **4** adopts a Type II conformation (ME_2PE_2) while a Type I conformation (M_2EM_2E) was also found as a reasonable option by calculations but not observed experimentally (Figure 3b). Conversely, the prevalent conformation of heptamer **5** (M_4EME) is of Type I and is related to a helix-loop structure. A Type I conformation is also predicted for the 8mer (M_4EM_2E, Figure 7a), but with large fluctuations in the M_2E segment, indicating its instability. We believe this instability comes from the mismatch of orientations of the *C* and *N*-termini of helix segment M_4 to the *N* and *C*-termini of helix segment M_2.

Secondly, in the macrocycle, the termini of the two helices are properly oriented with respect to each other. This orientation between the two termini in the helical plane is determined by the number of units and the intrinsic curvature angles of the Q units. Our study shows that M_1, M_4, M_6 and M_9 provide good termini orientation matches between helical segments,[25] whereas M_2 requires a distortion of the intrinsic curvature and is thus energetically unfavorable. This is possibly the reason why the M_2EM_2E conformation of **4** is less favorable than the ME_2PE_2 even though M_2EM_2E has fewer misfolds. In summary, the second structural rule limits the number of units involved in each helix segment to a few favorable cases that do not constrain the intrinsic curvature of Q units.

The third rule concerns the length match between the two helical segments. Two helical segments with same or similar number of units result in more stable structures, be they helix-loop or helix-helix structures. $M_4E_2PE_2$, $M_4E_2P_4E_2$, $M_6E_2P_4E_2$, and $M_6E_2P_6E_2$ (Figure 7b,c,d,e) are examples of this kind. Otherwise, a mismatch in length results in less prevalent populations, as for $M_6E_2PE_2$, $M_7E_2PE_2$, $M_6E_3ME_3$ and $M_9E_3ME_3$.

In helix-helix structures, i.e. when both helix segments span more than one turn, steric clashes would occur if a single E unit separates the helices because it is not long enough.[26] $M_xE_3M_yE_3$ (x,y > 2) conformations related to Type I are then encountered as, for example, $M_4E_3M_4E_3$ and $M_6E_3M_4E_3$. These sequences can also adopt Type II conformations $M_6E_2P_4E_2$ and $M_6E_2P_6E_2$, respectively (Figure 7d,e), i.e. conformations with fewer extended units, which is in principle more favorable. Nevertheless, the conformational analysis of **4** showed that the number of E units is not always the prevailing criterion to determine the most stable conformation. Type II conformers remain the most reasonable and common for a majority of macrocycles.

A few other situations worth mentioning were encountered in the context of these MD simulations. A reasonable conformation with three E segments (MEP_2EPE_2) was found for the 8mer. Most remarkably, MD annealing yielded no prevalent conformation for the 10mer. Multiple conformers were obtained of which none account for more than 33%. This ring size thus constitutes an intriguing candidate for experimental studies. The 15mer was not investigated. Being that it has five more units than the 10mer (exactly two full helix turns), it might run into the same type of conformational conflict.

Conclusion

We have extended our trimer,[7] tetramer[7] and pentamer,[17] series of synthesized and experimentally characterized cyclic Q_n oligomers to the hexamer and heptamer. Simulated annealing molecular dynamics allowed us to formulate general rules and to make reasonable predictions about the conformation behavior of longer homomeric macrocycles up to the 16mer. The conformations express the natural helicogenic behavior of the monomers and include flipped aryl-CO bonds to accommodate the frustration that arises from constraining a helix in a short macrocycle. Two ensembles of plausible conformations dominate, namely helix-helix and helix-loop conformations. The prevalent hexamer and heptamer conformations represent prototypes of the helix-helix and helix-loop motifs, respectively. Altogether, the combination of macrocyclization and strong folding propensity emerges as a powerful approach to access shapes that would be improbable in noncyclic precursors. Given the great variety of aromatic amino acid monomers that have been developed in the context of foldamer research, there is considerable potential to extend our approach and diversify macrocycle structures. Furthermore, fluxional behavior within the macrocycles was shown experimentally and computationally to follow privileged pathways. The introduction of a single fluorine atom in the heptameric macrocycle showed some bias between the seven conformers that would otherwise be degenerate. This hints at the possibility that different side chains or aryl substitutions may prevent fluxional behavior, favor one conformer only and allow for the display of a defined

array of functional groups. Progress along this line is currently being made and will be reported in due course.

Experimental Section

Molecular dynamics simulation setup: The general AMBER force field (GAFF),[27] with improved torsional parameters,[28] was used in all simulations. Each simulated system contains a macrocycle solvated by explicit chloroform molecules in a periodic box measuring 50 to 70 Å along each side. The systems were initially equilibrated for 1 ns at a constant temperature of 300 K and a pressure of 1 atm. This was followed by simulated annealing, in which systems go through multiple, 10 ns long cycles of heating, cooling, and constant temperature periods, at constant volume. To ensure sufficient conformational sampling, multiple simulations with different starting conformers for each macrocycle were carried out (Table 1). The systems were heated up to 800 K and cooled back down to 300 K for data collection. All simulations were carried out using the AMBER-18 package.[29]

Crystallographic data: Deposition numbers 2059866, 2059868, 2059869, 2059870, 2059871, and 2063705 contain the supplementary crystallographic data for this paper. These data are provided free of charge by the joint Cambridge Crystallographic Data Centre and Fachinformationszentrum Karlsruhe Access Structures service.

Acknowledgements

We thank Dr. S. Baba, Japan Synchrotron Radiation Research Institute (JASRI), for their help in data collection in the X-ray analysis. Synchrotron radiation experiments were performed at the BL38B1 station of SPring-8 with approval of JASRI (Proposal Nos. 2018B1425). Dr. B. Kauffmann is gratefully acknowledged for his help in crystallographic data collection of compound **5F**. Open access funding enabled and organized by Projekt DEAL.

Conflict of Interest

The authors declare no conflict of interest.

Keywords: *cis* amide · fluxionality · foldamer · macrocycle · strained structures

[1] V. Martí-Centelles, M. D. Pandey, M. I. Burguete, S. V. Luis, *Chem. Rev.* **2015**, *115*, 8736.
[2] a) Y. H. Lau, P. de Andrade, Y. Wu, D. R. Spring, *Chem. Soc. Rev.* **2015**, *44*, 91; b) L. D. Walensky, A. L. Kung, I. Escher, T. J. Malia, S. Barbuto, R. D. Wright, G. Wagner, G. L. Verdine, S. J. Korsmeyer, *Science* **2004**, *305*, 1466; c) A. M. Spokoyny, Y. Zou, J. J. Ling, H. Yu, Y.-S. Lin, B. L. Pentelute, *J. Am. Chem. Soc.* **2013**, *135*, 5946.
[3] a) Q. Xiao, D. S. Ashton, Z. B. Jones, K. P. Thompson, J. L. Price, *RSC Chem. Biol.* **2020**, *1*, 273; b) G. Bhardwaj, V. Khipple Mulligan, C. D. Bahl, J. M. Gilmore, P. J. Harvey, O. Cheneval, G. W. Buchko, S. V. S. R. K. Pulavarti, Q. Kaas, A. Eletsky, P.-S. Huang, W. A. Johnsen, P. Jr. Greisen, G. J. Rocklin, Y. Song, T. W. Linsky, A. Watkins, S. A. Rettie, X. Xu, L. P. Carter, R. Bonneau, J. M. Olson, E. Coutsias, C. E. Correnti, T. Szyperski, D. J. Craik, D. Baker, *Nature* **2016**, *538*, 329.
[4] a) R. Katoono, K. Kusaka, K. Fujiwara, T. Suzuki, *Chem. Asian J.* **2014**, *9*, 3182; b) Z. J. Kinney, V. C. Kirinda, C. S. Hartley, *Chem. Sci.* **2019**, *10*, 9057; c) V. C. Kirinda, C. Scott Hartley, *Chem. Sci.* **2021**, https://doi.org/10.1039/D1SC01270C; d) B. Liu, C. G. Pappas, E. Zangrando, N. Demitri, P. J. Chmielewski, S. Otto, *J. Am. Chem. Soc.* **2019**, *141*, 1685; e) C. G. Pappas, P. K. Mandal, B. Liu, B. Kauffmann, X. Miao, D. Komáromy, W. Hoffmann, C. Manz, R. Chang, K. Liu, K. Pagel, I. Huc, S. Otto, *Nat. Chem.* **2020**, *12*, 1180; f) C. Tsiamantas, X. de Hatten, C. Douat, B. Kauffmann, V. Maurizot, H. Ihara, M. Takafuji, N. Metzler-Nolte, I. Huc, *Angew. Chem. Int. Ed.* **2016**, *55*, 6848; *Angew. Chem.* **2016**, *128*, 6962; g) N. Ponnuswamy, F. B. L. Cougnon, J. M. Clough, G. D. Pantos, J. K. M. Sanders, *Science* **2012**, *338*, 783.
[5] a) S. Höger, *J. Polym. Sci. Part A* **1999**, *37*, 2685; b) W. Zhang, J. S. Moore, *Angew. Chem. Int. Ed.* **2006**, *45*, 4416; *Angew. Chem.* **2006**, *118*, 4524.
[6] a) W. Feng, K. Yamato, L. Q. Yang, J. Ferguson, L. J. Zhong, S. L. Zou, L. H. Yuan, X. C. Zeng, B. Gong, *J. Am. Chem. Soc.* **2009**, *131*, 2629; b) B. Gong, *Acc. Chem. Res.* **2008**, *41*, 1376; c) J. S. Ferguson, K. Yamato, R. Liu, L. He, X. C. Zeng, B. Gong, *Angew. Chem. Int. Ed.* **2009**, 48, 3150; *Angew. Chem.* **2009**, *121*, 3196; d) H. Fu, Y. Liu, H. Zeng, *Chem. Commun.* **2013**, *49*, 4127; e) Y. Liu, J. Shen, C. Sun, C. Ren, H. Zeng, *J. Am. Chem. Soc.* **2015**, *137*, 12055.
[7] H. Jiang, J.-M. Léger, P. Guionneau, I. Huc, *Org. Lett.* **2004**, *6*, 2985.
[8] a) L. Zang, Y. Che, J. S. Moore, *Acc. Chem. Res.* **2008**, *41*, 1596; b) L. Shua, M. Mayor, *Chem. Commun.* **2006**, 4134; c) Q. H. Wang, Y. L. Zhong, D. P. Miller, X. X. Lu, Q. Tang, Z. L. Lu, E. Zurek, R. Liu, B. Gong, *J. Am. Chem. Soc.* **2020**, *142*, 2915; d) Y. L. Zhong, Y. Yang, Y. Shen, W. W. Xu, Q. H. Wang, A. L. Connor, X. B. Zhou, L. He, X. C. Zeng, Z. F. Shao, Z. L. Lu, B. Gong, *J. Am. Chem. Soc.* **2017**, *139*, 15950; e) X. X. Wu, R. Liu, B. Sathyamoorthy, K. Yamato, G. X. Liang, L. Shen, S. F. Ma, D. K. Sukumaran, T. Szyperski, W. H. Fang, L. He, X. B. Chen, B. Gong, *J. Am. Chem. Soc.* **2015**, *137*, 5879.
[9] a) K. Tani, B. M. Stoltz, *Nature* **2006**, *441*, 731; b) J. Clayden, W. J. Moran, *Angew. Chem. Int. Ed.* **2006**, *45*, 7118; *Angew. Chem.* **2006**, *118*, 7276; c) A. J. Kirby, I. V. Komarov, P. D. Wothers, N. Feeder, *Angew. Chem. Int. Ed.* **1998**, *37*, 785; *Angew. Chem.* **1998**, *110*, 830.
[10] a) S. Yamago, Y. Watanabe, T. Iwamoto, *Angew. Chem. Int. Ed.* **2010**, *49*, 757; *Angew. Chem.* **2010**, *122*, 769; b) S. Mirzaei, E. Castro, R. Hernandez Sanchez, *Chem. Sci.* **2020**, *11*, 8089; c) N. K. Mitra, C. P. Merryman, B. L. Merner, *Synlett* **2017**, *28*, 2205.
[11] K. Miki, K. Ohe, *Chem. Eur. J.* **2020**, *26*, 2529.
[12] a) G. Povie, Y. Segawa, T. Nishihara, Y. Miyauchi, K. Itami, *Science* **2017**, *356*,172; b) Y. Segawa, M. Kuwayama, Y. Hijikata, M. Fushimi, T Nishihara, J. Pirillo, J. Shirasaki, N. Kubota, K. Itami, *Science* **2019**, *365*, 272; c) T.-H. Shi, Q.-H. Guo, S. Tong, M.-X. Wang, *J. Am. Chem. Soc.* **2020**, *142*, 4576.
[13] P. S. Bols, H. L. Anderson, *Acc. Chem. Res.* **2018**, *51*, 2083.
[14] a) I. Huc, *Eur. J. Org. Chem.* **2004**, *17*; b) D.-W. Zhang, X. Zhao, J.-Li Hou, Z.-T. Li, *Chem. Rev.* **2012**, *112*, 10, 5271.
[15] a) X. Ki, X. Yuan, P. Deng, L. Chen, Y. Ren, C. Wang, L. Wu, W. Feng, B. Gong, L. Yuan, *Chem. Sci.* **2017**, *8*, 2091; b) X. Li, B. Li, L. Chen, J. Hu, C. Wen, Q. Zheng, L. Wu, H. Zeng, B. Gong, L. Yuan, *Angew. Chem. Int. Ed.* **2015**, *54*, 11147; *Angew. Chem.* **2015**, *127*, 11299; c) Y. Yang, W. Feng, J. Hu, S. Zou, R. Gao, K. Yamato, M. Kline, Z. Cai, Y. Gao, Y. Wang, Y. Li, Y. Yang, L. Yuan, X. C. Zeng, B. Gong, *J. Am. Chem. Soc.* **2011**, *133*, 18590; d) B. Qin, C. Ren, R. Ye, C. Sun, K. Chiad, X. Chen, Z. Li, F. Xue, H. Su, G. A. Chass, H. Zeng, *J. Am. Chem. Soc.* **2010**, *132*, 9564; e) B. Qin, X. Chen, X. Fang, Y. Shu, Y. K. Yip, Y. Yan, S. Pan, W. Q. Ong, C. Ren, H. Su, H. Zeng, *Org. Lett.* **2008**, *10*, 5127; f) Y.-Y. Zhu, C. Li, G.-Y. Li, X.-K. Jiang, Z.-T. Li, *J. Org. Chem.* **2008**, *73*, 1745.
[16] a) H. Jiang, J.-M. Léger, I. Huc, *J. Am. Chem. Soc.* **2003**, *125*, 3448; b) C. Dolain, A. Grélard, M. Laguerre, H. Jiang, V. Maurizot, I. Huc, *Chem. Eur. J.* **2005**, *11*, 6135; c) T. Qi, V. Maurizot, H. Noguchi, T. Charoenraks, B. Kauffmann, M. Takafuji, H. Ihara, I. Huc, *Chem. Commun.* **2012**, *48*, 6337.
[17] K. Urushibara, Y. Ferrand, Z. Liu, H. Masu, V. Pophristic, A. Tanatani, I. Huc, *Angew. Chem. Int. Ed.* **2018**, *57*, 7888; *Angew. Chem.* **2018**, *130*, 8014.
[18] H. Jangra, M. H. Haindl, F. Achrainer, J. Hioe, R. M. Gschwind, H. Zipse, *Chem. Eur. J.* **2016**, *22*, 13328.
[19] a) F. Weygand, W. Steglich, J. Bjarnason, R. Akhtar, N. M. Khan, *Tetrahedron Lett.* **1966**, *7*, 3483; b) C. Hyde, T. Johnson, D. Owen, M. Quibell, R. Sheppard, *Int. J. Pept. Protein Res.* **1994**, *43*, 431.
[20] H. M. König, R. Abbel, D. Schollmeyer, A. F. M. Kilbinger, *Org. Lett.* **2006**, *8*, 1819.
[21] a) G. Fischer, *Chem. Soc. Rev.* **2000**, *29*, 119; b) B. F. Pedersen, B. Pedersen, *Tetrahedron Lett.* **1965**, 2995.
[22] a) J. Clayden, A. Lund, L. Vallverdú, M. Helliwell, *Nature* **2004**, *431*, 966; b) A. Tanatani, A. Yokoyama, I. Azumaya, Y. Takakura, C. Mitsui, M. Shiro, M. Uchiyama, A. Muranaka, N. Kobayashi, T. Yokozawa, *J. Am. Chem. Soc.* **2005**, *127*, 8553; c) M. Kudo, K. Katagiri, I. Azumaya, H. Kagechika, A.

Tanatani, *Tetrahedron* **2012**, *68*, 4455; d) K. Urushibara, H. Masu, H. Mori, I. Azumaya, T. Hirano, H. Kagechika, A. Tanatani, *J. Org. Chem.* **2018**, *83*, 14338.
[23] Even though no interconversion was observed between the ME_2PE_2 and M_2EM_2E conformers of **4**.
[24] A. M. Abramyan, Z. Liu, V. Pophristic, *Chem. Commun.* **2016**, *52*, 669.
[25] Note that M_6 and M_9 span exactly two more turns (five Q units) that M_1 and M_4, respectively and thus provide pairwise the same relative orientation of their termini.
[26] M_xEM_yE Type I conformations have been encountered in large cyclodextrins: K. Gessler, I. Usón, T. Takaha, N. Krauss, S. M. Smith, S. Okada, G. M. Sheldrick, W. Saenger, *Proc. Natl. Acad. Sci. USA* **1999**, *96*, 4246.
[27] J. Wang, R. M. Wolf, J. W. Caldwell, P. A. Kollman, D. A. Case, *J. Comput. Chem.* **2004**, *25*, 1157.
[28] Z. Liu, A. M. Abramyan, V. Pophristic, *New J. Chem.* **2015**, *39*, 3229.
[29] D. A. Case, I. Y. Ben-Shalom, S. R. Brozell, D. S. Cerutti, T. E. Cheatham, III, V. W. D. Cruzeiro, T. A. Darden, R. E. Duke, D. Ghoreishi, M. K. Gilson, H. Gohlke, A. W. Goetz, D. Greene, R Harris, N. Homeyer, Y. Huang, S. Izadi, A. Kovalenko, T. Kurtzman, T. S. Lee, S. LeGrand, P. Li, C. Lin, J. Liu, T. Luchko, R. Luo, D. J. Mermelstein, K. M. Merz, Y. Miao, G. Monard, C. Nguyen, H. Nguyen, I. Omelyan, A. Onufriev, F. Pan, R. Qi, D. R. Roe, A. Roitberg, C. Sagui, S. Schott-Verdugo, J. Shen, C. L. Simmerling, J. Smith, R. Salomon-Ferrer, J. Swails, R. C. Walker, J. Wang, H. Wei, R. M. Wolf, X. Wu, L. Xiao, D. M. York, P. A. Kollman (**2018**), AMBER 2018, University of California, San Francisco.

Manuscript received: April 3, 2021
Accepted manuscript online: April 27, 2021
Version of record online: May 27, 2021

